

Microscopic Study of Electronic and Magnetic Properties for Ir Oxide

Tomonori SHIRAKAWA*, Hiroshi WATANABE, and Seiji YUNOKI

Computational Condensed Matter Physics Laboratory, RIKEN ASI, Wako, Saitama 351-0198, Japan, CREST, Japan Science and Technology Agency (JST), Kawaguchi, Saitama 332-0012, Japan, and Computational Materials Science Research Team, RIKEN AICS, Kobe, Hyogo 650-0047, Japan

The exact diagonalization and the variational cluster approximation (VCA) are used to study the nature of a novel Mott insulator induced by a strong spin-orbit coupling for a two-dimensional three-band Hubbard model consisting of the t_{2g} manifold of $5d$ orbitals. To characterize the ground state, we introduce a local Kramer's doublet which can represent a state with effective angular momentum $J_{\text{eff}} = |\mathbf{S} - \mathbf{L}| = 1/2$ as well as spin $S = 1/2$. Our systematic study of the pseudo-spin structure factor defined by the Kramer's doublet shows that the $J_{\text{eff}} = 1/2$ Mott insulator is smoothly connected to the $S = 1/2$ Mott insulator. Using the Kramer's doublet as a variational state for the VCA, we examine the one-particle excitations for the Mott insulating phase. These results are compared with recent experiments on Sr_2IrO_4 .

KEYWORDS: $5d$ electrons, spin-orbit coupling, Mott insulator, three-band Hubbard model, variational cluster approximation

1. Introduction

$5d$ transition metal oxides have attracted much attention because of their unique properties caused by a strong spin-orbit coupling (SOC) λ for $5d$ transition elements. One of such materials is Sr_2IrO_4 in a layered perovskite structure of K_2NiF_4 type.^{1,2} While Sr_2IrO_4 was first synthesized more than fifty years ago,¹ it is only in 90's that its electronic properties has been studied systematically as an analogous system to high- T_c cuprate superconductors. An inelastic neutron scattering experiment has found that the ground state of Sr_2IrO_4 is antiferromagnetically ordered with weak ferromagnetic moment, similar to that for the parent compounds of cuprates.² The early studies then concluded that the ground state of Sr_2IrO_4 was a spin $S = 1/2$ Mott insulator with unpaired electrons occupying a half-filled d_{xy} band, which is split off upward compared to d_{yz} and d_{zx} orbitals due to the crystalline electrostatic field with elongation of the Ir-O bond along z direction.³ However, very recently, x-ray scattering experiments have revealed that the ground state is instead close to a $J_{\text{eff}} = 1/2$ Mott insulator.⁴ Here, $J_{\text{eff}} = |\mathbf{S} - \mathbf{L}|$ is an effective total angular momentum defined in the t_{2g} manifold with the orbital angular momentum \mathbf{L} . Note also that the $J_{\text{eff}} = 1/2$ state corresponds to the ground state in the atomic limit with large λ .

Motivated by these experiments, we shall study theoretically the electronic and magnetic properties of Sr_2IrO_4 using a three-band Hubbard model with the SOC.⁵ First, we introduce a local Kramer's doublet which can represent a $S = 1/2$ state as well as a $J_{\text{eff}} = 1/2$ state.⁶ Employing the exact diagonalization method, we show that the local Kramer's doublet can describe smoothly both the $S = 1/2$ and $J_{\text{eff}} = 1/2$ Mott insulators with varying λ . This strongly indicates that there exists no apparent symmetry change between

these two extreme states. We then employ the variational cluster approximation⁷ (VCA) method based on the self-energy functional theory⁸ (SFT) to examine the one-particle excitations in the Mott insulating phase. We find that, for a realistic set of model parameters for Sr_2IrO_4 , most of the unoccupied state, i.e., the upper Hubbard band, can be well describe by the $J_{\text{eff}} = 1/2$ state. This result is in good qualitative agreement with the recent experimental observation.⁴ We also discuss the effects of SOC and local Coulomb interactions on the one-particle excitations.

The paper is organized as follows. After describing the three-band Hubbard model in Sec. 2, the local Kramer's doublet is introduced in Sec. 3 and compared with the numerically exact ground state of the model. Using VCA based on SFT, the one-particle excitations are studied in Sec. 4. The paper is concluded in Sec. 5.

2. Model

Since the crystalline electrostatic field is much larger than the SOC and the local Coulomb interactions,¹⁰ the local electronic configuration of Ir^{4+} ion in Sr_2IrO_4 is the low-spin state of $(t_{2g})^5$. Therefore, we consider the following effective three-band Hubbard model, consisting of three d orbitals (d_{xy} , d_{yz} , and d_{zx}), on the square lattice

$$H = H_{\text{kin}} + H_{\text{so}} + H_{\text{int}} \quad (1)$$

$$H_{\text{kin}} = \sum_{\mathbf{k}\alpha\sigma} \epsilon_{\mathbf{k}}^\alpha c_{\mathbf{k}\alpha\sigma}^\dagger c_{\mathbf{k}\alpha\sigma} \quad (2)$$

$$H_{\text{so}} = \lambda \sum_{\mathbf{r}} \boldsymbol{\ell}_{\mathbf{r}} \cdot \mathbf{s}_{\mathbf{r}} \quad (3)$$

$$H_{\text{int}} = U \sum_{\mathbf{r}\alpha} n_{\mathbf{r}\alpha\uparrow} n_{\mathbf{r}\alpha\downarrow} + \frac{U'}{2} \sum_{\mathbf{r}\sigma} \sum_{\alpha \neq \beta} n_{\mathbf{r}\alpha\sigma} n_{\mathbf{r}\beta\sigma} + \frac{1}{2} (U' - J) \sum_{\mathbf{r}\sigma} \sum_{\alpha \neq \beta} n_{\mathbf{r}\alpha\sigma} n_{\mathbf{r}\beta\sigma}$$

* E-mail: t-shirakawa@riken.jp

Table I. Two sets of parameters used.

Parameters	Simplified model	Sr ₂ IrO ₄
t_1	0.36 eV	0.36 eV
t_2	0.00 eV	0.18 eV
t_3	0.00 eV	0.09 eV
t_4	0.36 eV	0.37 eV
t_5	0.00 eV	0.06 eV
Δ	0.36 eV	-0.36 eV
λ	—	0.37 eV

$$\begin{aligned}
& -J \sum_{\mathbf{r}} \sum_{\alpha \neq \beta} c_{\mathbf{r}\alpha\uparrow}^\dagger c_{\mathbf{r}\alpha\downarrow} c_{\mathbf{r}\beta\downarrow}^\dagger c_{\mathbf{r}\beta\uparrow} \\
& + J' \sum_{\mathbf{r}} \sum_{\alpha \neq \beta} c_{\mathbf{r}\alpha\uparrow}^\dagger c_{\mathbf{r}\alpha\downarrow}^\dagger c_{\mathbf{r}\beta\downarrow} c_{\mathbf{r}\beta\uparrow}.
\end{aligned} \quad (4)$$

Here, $c_{\mathbf{r}\alpha\sigma}$ ($c_{\mathbf{r}\alpha\sigma}^\dagger$) is the annihilation (creation) operator of an electron with spin σ ($\sigma = \uparrow, \downarrow$) and orbital α ($\alpha = xy, yz$, and zx) at site \mathbf{r} . $c_{\mathbf{k}\alpha\sigma}$ is the Fourier transform of $c_{\mathbf{r}\alpha\sigma}$. $\epsilon_{\mathbf{k}}^\alpha$ is the dispersion of orbital α

$$\begin{aligned}
\epsilon_{\mathbf{k}}^{xy} &= -2t_1(\cos k_x + \cos k_y) - t_2 \cos k_x \cos k_y \\
&\quad - 2t_3(\cos 2k_x + \cos 2k_y) + \Delta,
\end{aligned} \quad (5)$$

$$\epsilon_{\mathbf{k}}^{yz} = -2t_4 \cos k_y - 2t_5 \cos k_x, \quad (6)$$

$$\epsilon_{\mathbf{k}}^{zx} = -2t_4 \cos k_x - 2t_5 \cos k_y, \quad (7)$$

where t_1 , t_2 , and t_3 correspond to the hopping integrals for d_{xy} orbitals located at the nearest, next nearest, and third nearest neighbor sites, respectively. t_4 and t_5 are the nearest neighbor hopping integrals for d_{yz} (d_{zx}) orbital in y (x) and x (y) directions, respectively. Δ is an energy level difference between d_{xy} orbital and the other orbitals (d_{yz} and d_{zx}), which is naturally expected due to the large crystalline electrostatic field inducing tetragonal splitting. H_{so} is the SOC term represented in the following matrix form

$$\begin{aligned}
2\ell_{\mathbf{r}} \cdot \mathbf{s}_{\mathbf{r}} &= \sum_{\sigma} \left(c_{\mathbf{r}xy\bar{\sigma}}^\dagger, c_{\mathbf{r}yz\sigma}^\dagger, c_{\mathbf{r}zx\sigma}^\dagger \right) \times \\
&\quad \begin{pmatrix} 0 & -s & -i \\ -s & 0 & is \\ i & -is & 0 \end{pmatrix} \begin{pmatrix} c_{\mathbf{r}xy\bar{\sigma}} \\ c_{\mathbf{r}yz\sigma} \\ c_{\mathbf{r}zx\sigma} \end{pmatrix},
\end{aligned} \quad (8)$$

where $s = +1$ (-1) for $\sigma = \uparrow$ (\downarrow), and $\bar{\sigma}$ indicates the opposite spin of σ . Finally, we introduce, for the local Coulomb interactions, the intra-orbital (U) and the inter-orbital (U') Coulomb interactions, the Hund's coupling J , and the pair-hopping J' , with $U = U' + 2J$ and $J = J'$.⁹⁾ The number of electrons is set to be 5 per site.

As shown in Table I, we use two sets of parameters indicated by "Simplified model" and "Sr₂IrO₄". The parameter set "Sr₂IrO₄" is a realistic set of parameters determined by fitting the band dispersion obtained from the first principles calculations based on density functional theory.¹⁰⁾

3. Exact diagonalization study

First, we have obtained the phase diagram for the simplified model with $U/t_1 = 8$ and $J/U = 0.15$ using exact diagonalization technique for a 4-site cluster.

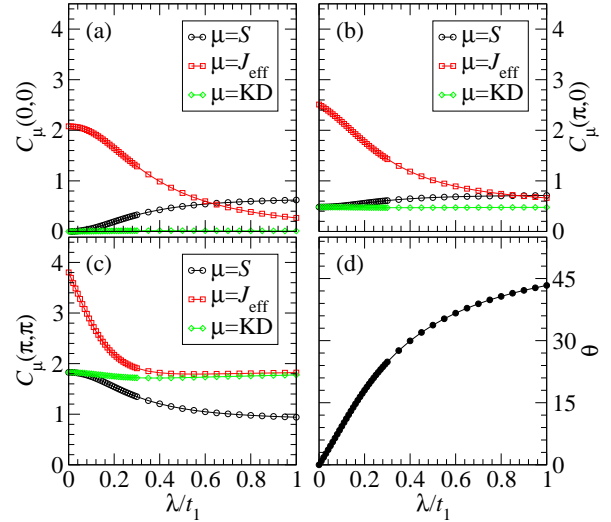


Fig. 1. (Color online) Structure factors $C_\mu(\mathbf{q})$ (for definition, see in the text) for (a) $\mathbf{q} = (0,0)$, (b) $\mathbf{q} = (\pi,0)$, and (c) $\mathbf{q} = (\pi,\pi)$. (d) The optimal value of θ for the Kramer's doublet [Eq. (9)]. The model parameters used are $U/t_1 = 8$, $J/U = 0.15$, $\Delta/t_1 = 1$, and the simplified hopping listed in Table I.

Let us briefly summarize the phase diagram of Δ vs. λ .¹¹⁾ In region (I) $\Delta/t_1 \lesssim -0.3$ and $\lambda/t_1 \lesssim 0.15$, d_{yz} and d_{zx} orbitals are magnetically active, whereas most of d_{xy} orbital is fully occupied. The degeneracy of d_{yz} and d_{zx} orbital leads to a ferromagnetic state with anti-ferro orbital ordering, which is expected by the second-order perturbation theory from the strong coupling limit in the presence of Hund's coupling.¹²⁾ In region (II) $-0.3 \lesssim \Delta/t_1 \lesssim 0.4$ and $\lambda/t_1 \lesssim 0.2$, the hole density is $n_{xy} : n_{yz} + n_{zx} = 1/2 : 1/2$ for $\lambda = 0$, and stripe-like spin correlations, characterized by $\mathbf{q} = (\pi,0)$ and $(0,\pi)$, become dominant. Finally, in region (III) $\Delta/t_1 \sim 1$ or $\lambda/t_1 \gtrsim 0.2$, an antiferromagnetic insulating phase appears, including both $S = 1/2$ and $J_{\text{eff}} = 1/2$ Mott insulators in the limit of $\lambda = 0$ and ∞ , respectively.

Let us now discuss closely the ground state properties in region (III). We first introduce the following local Kramer's doublet

$$a_{\mathbf{r}\theta\sigma}^\dagger = s \cos \theta c_{\mathbf{r}xy\sigma}^\dagger + \frac{\sin \theta}{\sqrt{2}} \left(c_{\mathbf{r}yz\bar{\sigma}}^\dagger + is c_{\mathbf{r}zx\bar{\sigma}}^\dagger \right), \quad (9)$$

which includes the two limiting states, namely, $S = 1/2$ (d_{xy}) for $\theta = 0$ and $J_{\text{eff}} = 1/2$ for $\theta = \arctan \sqrt{2} \sim 54.74^\circ$. In the atomic limit, the eigenstate of the highest level of H_{so} in the presence of Δ is generally expressed by this state.⁶⁾ Here, we shall optimize θ by minimizing the hole density $n_{\theta\sigma} = \langle \psi_0 | a_{\mathbf{r}\theta\sigma}^\dagger a_{\mathbf{r}\theta\sigma} | \psi_0 \rangle$. This quantity should be $n_{\theta\sigma} = 0.5$ if $a_{\mathbf{r}\theta\sigma}^\dagger$ is a well-defined particle. The numerically obtained optimized θ is summarized in Fig. 1 (d) for the simplified model, where we can see that the optimized θ varies smoothly with λ . The deviation of $n_{\theta\sigma}$ from 0.5 is found less than 1.2% for a range of λ studied, indicating that the ground state is well described by the Kramer's doublet.

Next, let us study the magnetic properties in region (III) of the phase diagram. For this purpose, we first

define the structure factor for a local angular momentum operator $\mathbf{O}_{\mathbf{r}}^{\mu}$

$$C_{\mu}(\mathbf{q}) = \frac{1}{N} \sum_{\mathbf{r}, \mathbf{r}'} e^{i\mathbf{q} \cdot (\mathbf{r} - \mathbf{r}')} \langle \psi_0 | \mathbf{O}_{\mathbf{r}}^{\mu} \cdot \mathbf{O}_{\mathbf{r}'}^{\mu} | \psi_0 \rangle, \quad (10)$$

where N is the number of lattice sites, and $|\psi_0\rangle$ indicates the ground state. The spin structure factor $C_S(\mathbf{q})$ is then obtained simply by setting

$$\mathbf{O}_{\mathbf{r}}^S = \mathbf{S}_{\mathbf{r}} = \frac{1}{2} \sum_{\alpha\alpha'\sigma\sigma'} c_{\mathbf{r}\alpha\sigma}^{\dagger} \boldsymbol{\sigma}_{\sigma\sigma'} c_{\mathbf{r}\alpha'\sigma'}, \quad (11)$$

where $\boldsymbol{\sigma}$ is the vector representation of Pauli matrices. The structure factor for the effective total angular momentum $C_{J_{\text{eff}}}(\mathbf{q})$ is defined by introducing the following local angular momentum operator

$$\mathbf{O}_{\mathbf{r}}^{J_{\text{eff}}} = \mathbf{S}_{\mathbf{r}} - \sum_{\alpha\alpha'\sigma} c_{\mathbf{r}\alpha\sigma}^{\dagger} \mathbf{L}_{\alpha\alpha'} c_{\mathbf{r}\alpha'\sigma}, \quad (12)$$

where \mathbf{L} is the orbital angular momentum operator. Note that as long as the local bases are confined within t_{2g} manifold, the matrix elements among t_{2g} states are equivalent to those among p states apart from minus sign.¹³⁾ Finally, we define the structure factor for the Kramer's doublet $C_{\text{KD}}(\mathbf{q})$ by introducing the following pseudo-spin 1/2 operator

$$\mathbf{O}_{\mathbf{r}}^{\text{KD}} = \frac{1}{2} \sum_{\sigma\sigma'} a_{\mathbf{r}\theta\sigma}^{\dagger} \boldsymbol{\sigma}_{\sigma\sigma'} a_{\mathbf{r}\theta\sigma'}, \quad (13)$$

where $a_{\mathbf{r}\theta\sigma}^{\dagger}$ is given in Eq. (9).

The numerical results for these structure factors are shown in Fig. 1. For $\lambda = 0$, the ground state is the $S = 1/2$ Mott insulator, where the hole density of d_{xy} orbital is exactly 1 whereby the model is equivalent to the single-band Hubbard model. With increasing λ , we can see in Fig. 1 (a)–(c) that the values of $C_{J_{\text{eff}}}(\mathbf{q})$ approach to those of $C_S(\mathbf{q})$ for $\lambda = 0$. This indicates that the ground state in the limit of large λ is represented simply by an antiferromagnetic ordering of $J_{\text{eff}} = 1/2$ angular momentum. Finally, we also find in Fig. 1 (a)–(c) almost no λ dependence on $C_{\text{KD}}(\mathbf{q})$, which strongly suggests that the ground state for different values of λ can be well described by a state with alternative alignment of the Kramer's doublet pseudo-spin. Therefore, we conclude that the $S = 1/2$ and $J_{\text{eff}} = 1/2$ Mott insulators, the two extreme states for $\lambda = 0$ and ∞ , are smoothly connected with no apparent symmetry change.

4. Variational Cluster Approximation Study

We now adopt the VCA method⁷⁾ based on the SFT⁸⁾ to study the low-energy one-particle excitations. This method takes into account precisely the effects of short-range static and dynamical correlations, and thus it is superior to a simple mean field approximation. The SFT introduces a reference Hamiltonian H' with the same two-body interactions as H but with a different one-body part \mathbf{t}' , and H' may be solved numerically exactly on a finite cluster. An approximate grand potential for H is given in a functional form by $\Omega(\mathbf{t}') = \Omega' - \text{Tr} \ln(-\hat{G}_0^{-1} + \hat{\Sigma}(\mathbf{t}')) + \text{Tr} \ln(-\hat{G}^{-1}(\mathbf{t}'))$, where Ω' ,

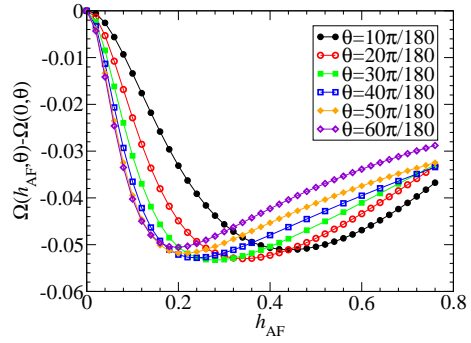


Fig. 2. (Color online) Variational parameter h_{AF} dependence of the grand potential for various values of θ [Eqs. (9) and (14)] for $U = 1.44$ eV, $J/U = 0.15$, and the realistic set of parameters for Sr_2IrO_4 listed in Table I.

$\hat{\Sigma}(\mathbf{t}')$, and $\hat{G}(\mathbf{t}')$ are the ground potential, self-energy, and Green's function of the reference system H' , respectively. \hat{G}_0 is the non-interacting Green's function of H . The variational condition $\partial\Omega(\mathbf{t}')/\partial\mathbf{t}' = 0$ determines an appropriate reference system H' which describes the original system H approximately.

To study the symmetry-broken long-range-ordered states in the VCA, we introduce suitably chosen fictitious Weiss fields in a set of variational parameters \mathbf{t}' . In this study, we introduce the Weiss field acting on the Kramer's doublet

$$H_{\text{AF}} = h_{\text{AF}} \sum_{\mathbf{r}\sigma} e^{i\mathbf{Q} \cdot \mathbf{r}} a_{\mathbf{r}\theta\sigma}^{\dagger} a_{\mathbf{r}\theta\bar{\sigma}}. \quad (14)$$

with $\mathbf{Q} = (\pi, \pi)$. Note that we only consider the Weiss field corresponding to the in-plane antiferromagnetic ordering since the energy for the states with the out-of-plane antiferromagnetic ordering is always higher than that for the in-plane one, as reported previously.⁵⁾

Fig. 2 shows $\Omega(h_{\text{AF}}, \theta) - \Omega(0, \theta)$ per site for different values of θ and with $U = 1.44$ eV, $J/U = 0.15$, and the realistic set of parameters for Sr_2IrO_4 listed in Table I. The fact that this quantity has a minimum at a finite value of h_{AF} indicates that the ground state is antiferromagnetically ordered. Carrying out careful calculations, we also find that the optimal value of θ is $\theta \approx 25^\circ$ for this set of model parameters.

Let us now study the one-particle excitations using the Green's function optimized above. The results for the momentum resolved one-particle excitation spectra and the density of states are shown in Fig. 3. Here, to understand the effects of λ as well as U , we choose three different sets of parameters with (a) and (d): $\lambda = U = J = 0$, (b) and (e): $\lambda = 0.37$ eV and $U = J = 0$, and (c) and (f): $\lambda = 0.37$ eV, $U = 1.44$ eV, and $J/U = 0.15$.

As clearly seen in Fig. 3 (a), when the SOC and the local Coulomb interactions are absent, the bands consist of two one-dimension-like narrower bands (ranging from -1 eV to 0 eV), which are originated from d_{yz} and d_{zx} orbitals, and the remaining band with broader band width extending from -3.2 eV to 0.5 eV, which has a characteristic of d_{xy} . As shown in Fig. 3 (d), the projected density of states onto $J_{\text{eff}} = 1/2$ extends to the

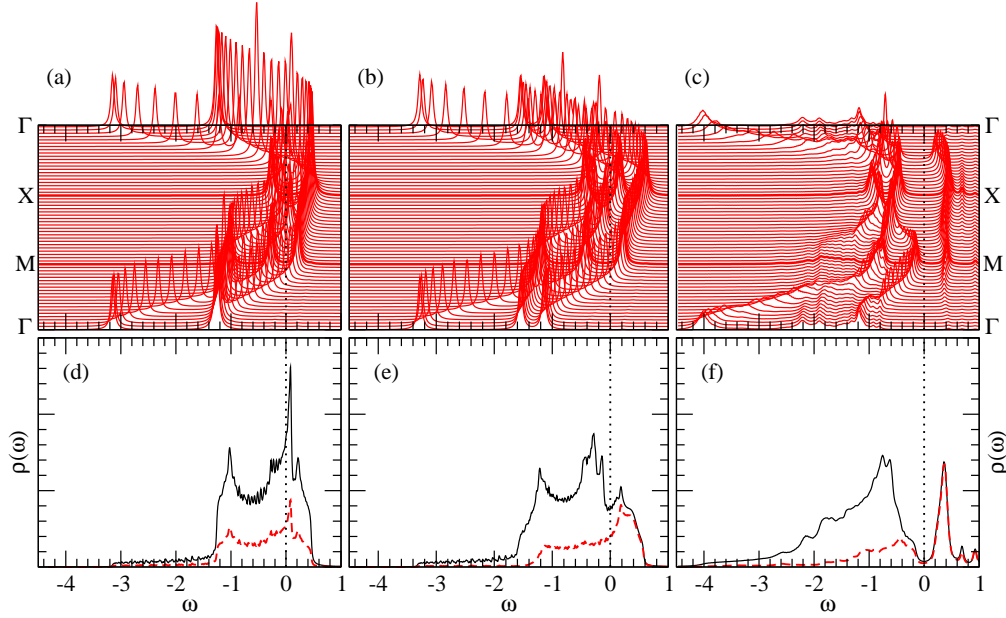


Fig. 3. (Color online) The momentum resolved one-particle excitation spectra (upper panels) and the density of states $\rho(\omega)$ (lower panels) for (a) and (d): $\lambda = U = J = 0$, (b) and (e): $\lambda = 0.37$ eV and $U = J = 0$, and (c) and (f): $\lambda = 0.37$ eV, $U = 1.44$ eV and $J/U = 0.15$. Other parameters used are the realistic ones for Sr_2IrO_4 listed in Table I. Γ , M and X correspond to $(k_x, k_y) = (0, 0)$, $(\pi, 0)$, and (π, π) in first Brillouin zone, respectively. In (d), (e), and (f), black solid (red dashed) lines indicate the total density of states (the partial density of states projected onto $J_{\text{eff}} = 1/2$). $\omega = 0$ corresponds to the Fermi level. Delta functions are represented using Lorentzian functions with its half-width at half-maximum $\eta = 0.1t_1$ for (a), (b), and (c), and $\eta = 0.005t_1$ for (d), (e), and (f).

whole energy band, indicating that $J_{\text{eff}} = 1/2$ is not a good quantity to describe the one-particle excitations. When the SOC is turned on in Fig. 3 (b) and (e), the three different bands are observed, i.e., the highest one located from -1.1 to 0.6 eV in energy, the intermediate one ranging from -1.4 to 0.2 eV, and the lowest one extending from -3.2 to -0.2 eV. For this case, we can observe that while the partial density of states projected onto $J_{\text{eff}} = 1/2$ is still extended to the whole energy region, most of the unoccupied states (from ~ 0.2 to ~ 0.6 eV) has a characteristic of $J_{\text{eff}} = 1/2$. Finally, when we include the Coulomb interactions in Fig. 3 (c) and (f), we can clearly see that the “upper Hubbard band”, which is located above the Fermi level, is well separated from the valence band. We can also see in Fig. 3 (f) that almost all the unoccupied states is of $J_{\text{eff}} = 1/2$ characteristic, which provides a numerical evidence that the ground state is well characterized by the $J_{\text{eff}} = 1/2$ Mott insulator. This finding is in good qualitative agreement with the recent experiments on Sr_2IrO_4 .⁴⁾

5. Conclusions

We have employed the exact diagonalization method to study the ground state phase diagram for the three-band Hubbard model with the SOC. We have found that in the Mott insulating phase the ground state can be well described by the Kramer’s doublet. This suggests that no apparent symmetry change exists between the two extreme states, i.e., the $S = 1/2$ Mott insulator and the $J_{\text{eff}} = 1/2$ Mott insulator, which appear for $\lambda = 0$ and ∞ , respectively. We have also studied the one-particle excitations using the VCA, and found that both λ and

U are essential to realize the $J_{\text{eff}} = 1/2$ Mott insulator, where the unoccupied states are mostly of $J_{\text{eff}} = 1/2$ characteristic.

Acknowledgment

The authors thank J. Matsuno and H. Onishi for useful discussions. Most of the computation has been done using the RIKEN Cluster of Clusters (RICC) facility.

- 1) J. J. Randall Jr., L. Katz, and R. Ward: J. Am. Chem. Soc. **79** (1957) 266.
- 2) M. K. Crawford, M. A. Subramanian, R. L. Harlow, J. A. Fernandez-Baca, Z. R. Wang, and D. C. Johnston: Phys. Rev. B **49** (1994).
- 3) G. Cao, J. Bolivar, S. McCall, J. E. Crow, and R. P. Guertin: Phys. Rev. B **57** (1998) 11039.
- 4) B. J. Kim, H. Ohsumi, T. Komesu, S. Sakai, T. Morita, H. Takagi, and T. Arima: Science **323** (2009) 1329.
- 5) H. Watanabe, T. Shirakawa, and S. Yunoki: Phys. Rev. Lett. **105** (2010) 216410.
- 6) G. Jackeli and G. Khaliullin: Phys. Rev. Lett. **102** (2009) 017205.
- 7) M. Potthoff, M. Aichhorn, and C. Dahnken: Phys. Rev. Lett. **91** (2003) 206402.
- 8) M. Potthoff: Eur. Phys. J. B **32** (2003) 429.
- 9) J. Kanamori: Prog. Theor. Phys. **30** (1963) 275.
- 10) H. Jin, H. Jeong, T. Ozaki, and J. Yu: Phys. Rev. B **80** (2009) 075112.
- 11) For details of the phase diagram, see T. Shirakawa *et al.*, to be published.
- 12) K. I. Kugel and D. I. Khomskii: Sov. Phys. JETP **37** (1973) 725.
- 13) S. Sugano, Y. Tanabe, and H. Kamimura: *Multiplets of Transition-Metal Ions in Crystals* (Academic Press, New York, USA, 1970).